Monthly Notices of the ROYAL ASTRONOMICAL SOCIETY

MNRAS **521,** 1620–1632 (2023) https://doi.org/10.1093/mnras/stac3703
Advance Access publication 2023 January 17

The Extragalactic Serendipitous Swift Survey (ExSeSS) – I. Survey definition and measurements of the X-ray number counts

Jack N. Delaney,[1]★ James Aird ,[1,2] Phil A. Evans ,[2] Cassandra Barlow-Hall,[1] Julian P. Osborne [2] and Michael G. Watson[2]

[1]*Institute for Astronomy, University of Edinburgh, Royal Observatory, Blackford Hill, Edinburgh EH9 3HJ, UK*
[2]*School of Physics and Astronomy, University of Leicester, University Rd, Leicester LE1 7RH, UK*

Accepted 2022 November 23. Received 2022 November 23; in original form 2022 July 28

ABSTRACT

We present the Extragalactic Serendipitous Swift Survey (ExSeSS), providing a new well-defined sample constructed from the observations performed using the Swift X-ray Telescope. The ExSeSS sample consists of 79 342 sources detected in the medium (1–2 keV), hard (2–10 keV), or total (0.3–10 keV) energy bands, covering 2086.6 deg^2 of sky across a flux range of $f_{0.3-10\,\mathrm{keV}} \sim 10^{-15} - 10^{-10}$ erg s^{-1} cm^{-2}. Using the new ExSeSS sample we present measurements of the differential number counts of X-ray sources as a function of 2–10 keV flux that trace the population of Active Galactic Nuclei (AGNs) in a previously unexplored regime. We find that taking the line-of-sight absorption column density into account has an effect on the differential number count measurements and is vital to obtain agreement with previous results. In the hard band, we obtain a good agreement between the ExSeSS measurements and previous, higher energy data from *NuSTAR* and *Swift*/BAT when taking into account the varying column density of the ExSeSS sample as well as the X-ray spectral parameters of each of the samples we are comparing to. We also find discrepancies between the ExSeSS measurements and AGN population synthesis models, indicating a change in the properties of the AGN population over this flux range that is not fully described by current models at these energies, hinting at a larger, moderately obscured population at low redshifts ($z \lesssim 0.2$) that the models are not currently taking into account.

Key words: galaxies: active – X-rays: galaxies.

1 INTRODUCTION

Active Galactic Nuclei (AGNs) occur when the supermassive black hole (SMBH) at the centre of a galaxy is rapidly accreting dust and gas, emitting large amounts of energy across the electromagnetic spectrum. Identifying AGN at X-ray wavelengths is particularly effective as the X-ray emission is able to penetrate surrounding material, allowing obscured sources that would not be found at other wavelengths to be identified (Brandt & Alexander 2015; Netzer 2015; Hickox & Alexander 2018). Observing in the X-ray band also enables the identification of low-luminosity AGN that would be too faint and diluted by the host galaxy light at other wavelengths. Finally, the vast majority of detected point sources in X-ray surveys are associated with AGN. All these factors make X-ray surveys ideal for identifying SMBHs in their growth phase as an AGN.

Since X-rays provide an extremely efficient way of probing the AGN population, significant efforts have been dedicated to a variety of different surveys. *ROSAT* (Trümper 1982) performed the first all-sky survey over the 0.1–2 keV energy band with the sensitivity of a focusing X-ray telescope, identifying over 100 000 sources (Voges et al. 2000; Boller et al. 2016). The *eROSITA* instrument on the Specktrum Roentgen-Gamma mission launched in 2019 has carried out a new, high-sensitivity all-sky X-ray survey at 0.2–8 keV, repeatedly scanning the sky every 6 months and is expected to detect >3 million AGNs, with the majority identified in the most sensitive, soft energy band (0.2–2.3 keV; Merloni et al. 2012; Predehl et al. 2021).

While *ROSAT* and *eROSITA* probe the whole sky, *Chandra* and *XMM-Newton* enable much deeper surveys over smaller areas. In particular, *Chandra* has carried out surveys ranging from ∼200 ks to 7 Ms depth over fields of ∼0.1–0.6 deg^2 (Alexander et al. 2003; Laird et al. 2009; Xue et al. 2011; Nandra et al. 2015; Zheng et al. 2017; Kocevski et al. 2018). The deepest *Chandra* survey, the Chandra Deep Field South (CDF-S: Luo et al. 2016) covers 484.2 arcmin^2 for 7 Ms of exposure with a total of 1008 sources detected across multiple energy bands, reaching an X-ray point source density of $\sim$ 23 900 deg^{-2} for AGN. These deep fields are complemented by wider area, shallower surveys including the ∼2 deg^2 COSMOS-Legacy survey (reaching ∼160 ks depth per pointing and containing ∼4000 sources: Civano et al. 2016) and the 9.3 deg^2 *Chandra* Deep Wide Field Survey (CDWF-S, reaching ∼30 ks depth per pointing with a total of 6891 sources: Masini et al. 2020). *XMM–Newton* has a larger collecting area and a wider field-of-view, but lacks the angular resolution of *Chandra*, so instead efforts have focused on performing shallower surveys over larger areas of sky (e.g. the ∼50 deg^2 XMM-XXL survey: Pierre et al. 2016).

In addition to these dedicated survey efforts, extremely large X-ray samples can also be constructed using sources found in the field-of-view during observations of dedicated targets with a different science objective. The large field-of-view of *XMM–Newton* makes it especially suitable for constructing such samples (e.g. 2XMM: Watson et al. 2009; 3XMM: Rosen et al. 2016) with the latest

★ E-mail: delaney@roe.ac.uk

compilation (4XMM: Webb et al. 2020) containing 550 124 X-ray sources and covering a total sky area of ∼1152 deg^2. A similar effort, the *Chandra* Source Catalog (CSC: Evans et al. 2010; Brown et al. 2019) contains a total of 315 000 source covering a total area of ∼550 deg^2 in its latest release.[1] However, 4XMM and CSC contain both sources associated with the targets of the observation and serendipitously detected sources within the field-of-view. We note that a key challenge in the analysis of these X-ray catalogues is the identification and removal of any X-ray sources that are associated with the target to construct a truly serendipitous sample. Mateos et al. (2008) describes the process of making an extragalactic serendipitous sample using 2XMM, producing a catalogue of 1129 *XMM–Newton* sources from a total sky area of 132.3 deg^2.

While sensitive surveys at soft X-ray energies ($\lesssim$ 2 keV) predominantly identify unobscured AGN, surveys at harder energies (∼2–10 keV) are able to identify both low and moderately obscured sources, although remain biased against the most heavily obscured (Compton-thick) sources. Surveys at even higher X-ray energies (>10 keV) are less biased against such populations. The Burst Alert Telescope (BAT) on the *Neil Gehrels Swift Observatory* (hereafter *Swift*; Barthelmy et al. 2005) is sensitive to an energy range of 15–150 keV and is constantly observing a large fraction of the sky to identify gamma ray bursts (GRBs) and measure their positions on the sky to ∼4-arcmin accuracy. Oh et al. (2018) present the most recent (105 month) catalogue containing 1632 persistent hard X-ray sources identified in the 14–195 keV energy band. However, *Swift*/BAT only detects the brightest sources in the local Universe due to its comparatively poor angular resolution and limited sensitivity. The *Nuclear Spectroscopic Telescope Array* (*NuSTAR*) X-ray Observatory, launched in 2012, was the first mission with grazing-incidence mirrors capable of focusing high-energy (∼10–80 keV) X-rays (Harrison et al. 2013; Madsen et al. 2015), enabling surveys that detect much fainter sources at these energies, albeit over substantially smaller areas of sky (∼0.3–1.7 deg^2, see Civano et al. 2015; Mullaney et al. 2015; Masini et al. 2018). To access larger areas of sky, Lansbury et al. (2017) constructed a catalogue of 497 truly serendipitous sources (i.e. excluding targets) in the 3–24, 3–8, or 8–24 keV bands using a compilation of the first 40 months of *NuSTAR* observations, covering a total sky area of ∼16 deg^2 (see also Alexander et al. 2013).

As X-ray point source samples in high Galactic latitude fields will be dominated by distant AGN, the most immediate quantification that an X-ray survey can provide – the number counts of sources in a given energy band at different fluxes – already places important constraints on the AGN population. To constrain the intrinsic X-ray source density as a function of flux (also referred to as the 'logN-logS') requires a combination of deep, small-area surveys and wide, shallow surveys to probe a wide range of fluxes, as well as an accurate quantification of the sensitivity of the X-ray observations. Measurements with *Chandra* and *XMM–Newton* have shown that the logN-logS is well described by a broken power-law over a broad range in flux, with a steep slope at brighter fluxes and a shallower slope at fluxes $\lesssim 10^{-14}$ erg s^{-1} cm^{-2} (e.g. Georgakakis et al. 2008; Mateos et al. 2008). With additional data – most crucially redshifts of the X-ray sources – our observational picture can be expanded to include the luminosity function and its evolution (e.g. Ueda et al. 2014; Aird et al. 2015). By incorporating constraints on the fraction of sources with different levels of absorption, a full 'population synthesis model' of AGN can be constructed that describes the evolution of AGN over cosmic time (e.g. Gilli, Comastri & Hasinger 2007; Ballantyne 2014) and can be tested using new measurements of the number counts in different energy bands. Harrison et al. (2016) presented the first measurements of the X-ray source number counts based on the *NuSTAR* surveys, including both the dedicated survey fields and the serendipitous sample from Lansbury et al. (2017). They found that the *NuSTAR* 8–24 keV logN-logS agrees well at fluxes $\sim 10^{-14} - 10^{-12}$ erg s^{-1} cm^{-2} with the predictions of population synthesis models that are based on earlier studies with *Chandra* and *XMM–Newton*. However, the *NuSTAR* number counts exceed the simplest extrapolation of the *Swift/BAT* number counts at brighter fluxes and – most notably – the *Swift*/BAT number counts do not agree with the population synthesis models that are successful at fainter fluxes, suggesting evolution of the AGN population between the higher redshifts sampled by *NuSTAR* and the local Universe sampled by *Swift*/BAT that is not fully captured in these models. However there have been few X-ray surveys that cover large enough area to directly probe the flux range spanning between the *NuSTAR* and *Swift*/BAT surveys, either at the same high energies ($\gtrsim$ 10 keV) or more moderate energies (∼2–10 keV) to help resolve this discrepancy.

In this paper, we present the Extragalactic Serendipitous Swift Survey (ExSeSS), a new sample of truly serendipitous sources at high Galactic latitudes and covering an area of 2086.6 deg^2 which is constructed from observations carried out with the *Swift* X-ray telescope (XRT). Our sample is extracted from the second *Swift* X-ray Point Source catalogue (2SXPS: Evans et al. 2020) which contains all sources detected in the 0.3–1, 1–2, 2–10, and 0.3–10 keV range, which we reduce to be primarily extragalactic (by excluding Galactic latitudes $-20^\circ < b < 20^\circ$) and serendipitous to provide an unbiased sample of X-ray sources to study the AGN population. In Section 2 we define the ExSeSS sample, describing the process to select the appropriate fields, identify and remove sources associated with the targets of the observations, create the source sample, and determine the overall area coverage and sensitivity. The ExSeSS source catalogue is described in Appendix A and made available online at TBD. In Section 3 we use the ExSeSS sample to measure the logN-logS with a particular focus on the 2–10 keV band where we probe a key flux range between *NuSTAR* and *Swift*/BAT, albeit at lower energies. We also compare ExSeSS to the established population synthesis models from Gilli et al. (2007), Ueda et al. (2014), and the updated model from Ballantyne (2014) as presented in Harrison et al. (2016). Our results provide new insights to help understand the obscuration properties of the AGN over this important flux range. In Section 4 we provide a summary of our work and conclusions, as well as discussing the usefulness of the ExSeSS sample for future studies.

2 SWIFT DATA AND DEFINITION OF THE EXSESS SAMPLE

The sources included in this paper are taken from the second *Swift* X-ray Point Source catalogue (2SXPS: Evans et al. 2020) which we have reduced to construct the ExSeSS sample. This process involved taking the full 3790 deg^2 covered by 2SXPS, removing areas covered by the Galactic plane or large nearby galaxies so that the sample is dominated by background extragalactic sources, and removing any X-ray sources associated with the targets from the resulting catalogues so that only truly serendipitous detections are retained. We describe the process to construct the ExSeSS sample and our method to define the area coverage (to different flux limits) covered by our new survey.

[1] https://cxc.cfa.harvard.edu/csc/char.html

2.1 *Swift*/XRT data

The 2SXPS data consist of a list of data sets, which correspond to the individual observations carried out by *Swift*/XRT, and a list of detections, which contain the thousands of sources that are detected in the different observations and in different energy bands (thus, in some cases, containing multiple detections of the same source). Each data set covers a region with a diameter of ∼23.6 arcmin, corresponding to the *Swift*/XRT field-of-view. Additional data sets were also generated by stacking the individual observations where overlapping areas of the sky have been viewed multiple times. This stacking improves the sensitivity in that area, revealing fainter sources and increasing the number of sources in the catalogue. In total in 2SXPS there are 143 697 data sets containing 1091 058 independent detections in either the 0.3–10 keV (total), 0.3–1 keV (soft), 1–2 keV (medium), or 2–10 keV (hard) energy bands, corresponding to 206 335 distinct sources and reaching down to flux limits of $f_{0.3-10\,\mathrm{keV}} \sim 10^{-14}$ erg cm^{-2} s^{-1} (Evans et al. 2020).

2.2 Construction of the ExSeSS sample

2.2.1 Defining the ExSeSS fields

Defining ExSeSS involves selecting the fields (and corresponding 2SXPS data sets) to include. We started by removing all the data sets that go in to a stacked data set, i.e. the individual data sets that have been observed over roughly the same area of sky that were combined to form a stacked data set. We retained the stacked data sets, corresponding to the deepest available data for a given area of sky, ensuring that we do not duplicate areas where multiple data sets cover the same location and that we have a well-defined sensitivity in these areas. Once this is done we are left with stacked data sets and the remaining unstacked data sets that are never used in a stack. Keeping both of these we have 18 640 data sets left in our sample.

Any data sets within 2SXPS that contain diffuse emission were removed, as well as data sets with significant stray light or containing very bright sources with fitting issues, which is indicated by a 'Field Flag' not equal to zero in 2SXPS, leaving us with 17 514 data sets. We also removed any data sets that lie within the Galactic plane (Galactic latitudes $-20^\circ < b < 20^\circ$) to ensure our sample is dominated by extragalactic X-ray sources. Next, we removed any data sets that fall within the sky area of a number of well-known nearby objects: the Small and Large Magellanic Clouds (SMC and LMC); M31 and M33. These were selected as they are relatively close to our galaxy and have well-known sizes. These objects are likely to contain many individually resolved X-ray sources such as stars and X-ray binaries (XRBs) which we do not want in our final sample. Our final list consists of 11 047 data sets that are retained in ExSeSS and hereafter referred to as the ExSeSS 'fields' (i.e. the areas of sky that form the ExSeSS survey). Table 1 summarizes the definition of the ExSeSS fields, while Fig. 1 shows the distribution of these fields across the sky compared to the original 2SXPS data sets.

2.2.2 Identifying Swift targets for exclusion from the ExSeSS sample

To create a truly serendipitous sample of sources requires that we identify the targets of the *Swift*/XRT observations corresponding to each of our data sets and subsequently remove any X-ray sources associated with these targets. The majority of our targets were identified using the data base maintained by Pennsylvania State University,[2] which provides a list of the known targets of pointed observations. We also removed GRB afterglows[3] that were identified using *Swift*/XRT following triggered observations. The number of targets identified from this process are given in Table 2. Astronomical objects corresponding to these targets were then extracted from the SIMBAD[4] data base using a closest match to find the angular size of the targets on the sky. We adopt the major axis of the object as provided by SIMBAD as an estimate of the target's radius.

We manually checked all targets with a radius larger than 10 arcmin to make sure that our SIMBAD cross-matching was identifying the correct target and found that in the majority of cases that the target did indeed have a large angular size (e.g. the M15 globular cluster or the M101 pair of galaxies were identified as targets, which contain multiple X-ray sources within the target radius that should be completely removed from our serendipitous source sample). However there were 14 targets that were erroneously associated with an object with an extremely large angular size that is unlikely to correspond to an X-ray source or *Swift* target (e.g. the Fermi bubble or nebula gas clouds). For these sources the true target could easily be identified with SIMBAD and they were manually updated.

Finally, we checked fields where no targets had been identified in the Pennsylvania State data base. Overall there were 7526 data sets that did not have a target associated with them following our initial analysis. To tackle this, we first identified the data sets that have zero detections and checked their exposure times. We thus identified 4886 relatively shallow data sets with no source detections. These fields correspond to observations where *Swift* was tracking an object, such as a comet, for a short amount of time across the sky. These fields are still very useful as they build up our overall sky coverage and are therefore kept in ExSeSS. After this we were still left with 2640 data sets with detections but no associated targets. For these remaining data sets we examined the name assigned to the observation by the original observers and were able to identify a target on this basis. In many cases, the target name was written in a non-standard format, requiring manual intervention to identify the correct target. Other issues included follow-up of sources from the *Swift*/BAT catalogue where we updated to the counterpart position from Oh et al. (2018).[5]

Table 1. Number of 2SXPS data sets that remain after applying each of the steps described in Section 2.2.1. Originally there were 143 697 data sets in the 2SXPS sample. We remove individual data sets that are incorporated into the stacked fields, leaving us with 18 640 unique sky pointings. After applying the 'Field Flag' to only use fields with good quality data we are left with 17 514 data sets. When removing the large objects (Galactic plane, SMC, LMC, M31, M33) we are left with 11 047 data sets, hereafter referred to as the 'ExSeSS fields'. In Section 2.2.2 if a target is larger than *Swifts* field of view then the data set will also be removed.

ExSeSS fields	
Fields type	Number of data sets remaining
2SXPS original	143 697
Unique sky pointings	18 640
Good field flag	17 514
Large objects removed	11 047

[2] https://www.swift.psu.edu/too_api/
[3] https://www.swift.ac.uk/xrt_positions
[4] http://simbad.u-strasbg.fr/simbad/sim-fbasic
[5] https://swift.gsfc.nasa.gov/results/bs105mon/

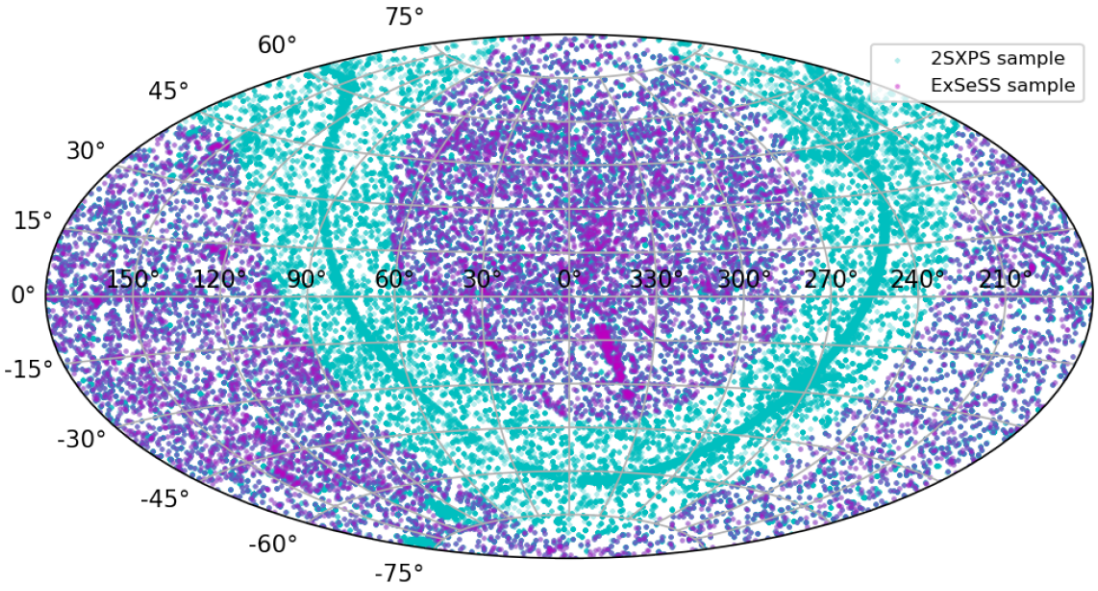

Figure 1. A map showing the distribution of the ExSeSS fields across the sky in right ascension and declination compared to the original 2SXPS. The 2SXPS data sets are shown in cyan and are distributed evenly over most of the sky. The ExSeSS fields are highlighted in purple and exclude the Galactic plane as well as areas of the sky such as the SMC and LMC. The process to define the ExSeSS fields is described in Section 2.2.1.

Table 2. Number of targets of *Swift*/XRT observations that are identified via different routes. The largest number of targets are identified from Penn State data base. Additional targets were identified from the list of known GRB afterglows that were the subject of *Swift*/XRT follow-up. Finally, we manually identified an additional 1007 targets based on the target name recorded by the original observers. In total there are 12 224 targets to be excluded from ExSeSS to make the sample serendipitous. There are an additional 5863 data sets that lack a defined target or contain no source detections and we do not assign a target.

Targets identified	
Target list	No. of targets
Penn State target data base	10 561
GRB afterglows	656
Manually identified based on target name	1007
Total no. of targets	12 224
Empty data sets not assigned targets	4886
Data sets without a defined target	977

We caution that in a number of cases the target does not fall at the nominal pointing position. Based on these manual checks, we identified 1007 extra targets to remove from 2SXPS to ensure a serendipitous sample, including the 14 that were identified in the Penn State data base but were initially associated with a counterpart with angular size >10 arcmin. We then followed the same process of identifying a SIMBAD counterpart to determine the angular size of the additional targets and added these to our list of targets and sky areas to exclude from ExSeSS.

Of the remaining 977 data sets that still lacked targets, twelve corresponded to dedicated survey fields such as COSMOS (thus all sources can be treated as serendipitous detections) and the rest were 'cooling' or 'offset' pointings (where *Swift* is purposefully pointed at a blank field position) or there was no other clearly defined target for the observation. These data sets are retained in ExSeSS but are not assigned a target. Thus, our final ExSeSS data consists of 11 047 fields (defined in Section 2.2.1 above) with 12 224 targets to be removed. We have more targets than data sets because of the stacked data sets, which are made up of a combination of pointings, each with their own individual targets, and therefore one stacked data set can have multiple targets within it.

2.2.3 *Defining the ExSeSS sources*

Our next step was to determine which X-ray detections from within the much larger catalogue provided by 2SXPS should be included in the ExSeSS sample of sources. First, we extracted only those 2SXPS detections that are associated with the refined list of ExSeSS fields, as described in Section 2.2.1 above, ensuring that our sample was dominated by extragalactic sources. Indeed, we expect our sample to be dominated by distant AGN (based on extrapolations of the X-ray number counts of different non-AGN populations from Lehmer et al. 2012, see also Section 3 below), although detailed cross-matching and classification using multiwavelength data (deferred to a future work) is required to confirm the level of contamination. At this stage, we also limited our sample to 'good' detections in the 2SXPS catalogue, which reduces the false detection rate to 0.3 per cent (see Evans et al. 2020, for more details). Where the edges of fields overlap some duplicate sources remain; in these cases we retained the detection with the highest exposure.

To ensure that our sample is serendipitous, we must remove any detected sources that are associated with the target of an observation, which would otherwise severely bias our sample. We removed any X-ray detections that lie within a radius of a target object corresponding to the angular size (as defined in Section 2.2.2 above) and thus ensured that sources that are associated with the target do not contaminate our sample. We also apply a conservative minimum radius of 2 arcmin to prevent any contamination from detections of the target source itself or spurious detections in the wings of bright targets. The process for creating the ExSeSS sample is summarized in Fig. 2 as a flow diagram to illustrate the process of taking the 2SXPS sample and refining it to construct the ExSeSS sample.

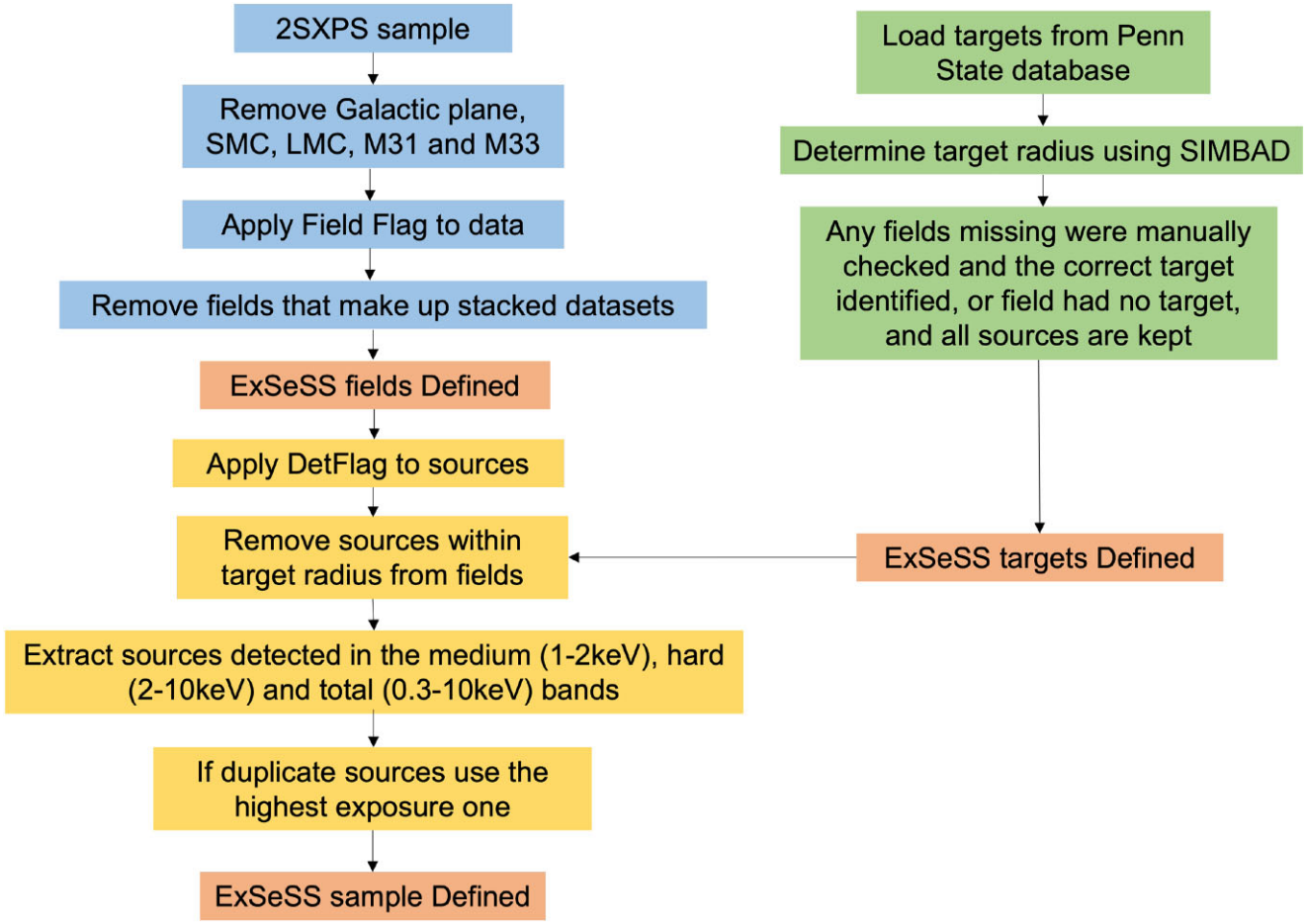

Figure 2. A flow diagram showing the process to create the ExSeSS sample from the 2SXPS data. In blue is the process used to define the ExSeSS fields and ensure the sample is dominated by distant, extragalactic sources. In green is the process to identify the targets of *Swift*/XRT observations and determine their angular sizes. The yellow boxes show the process to define the ExSeSS source sample and ensure it contains only serendipitous detections. The orange boxes indicate the key outputs from the process: the list of fields, the list of targets, and the final ExSeSS source sample. The process is explained in more detail in Section 2.2.

Finally, we limited our sample to sources detected in the medium (1–2 keV), hard (2–10 keV), or total (0.3–10 keV) bands from 2SXPS leaving us with a total of 79 342 sources in the ExSeSS sample. We converted the rates in the individual bands into fluxes assuming a simple power-law X-ray spectrum with a photon index of $\Gamma = 1.9$ and correcting for Galactic absorption with $N_{\rm H} = 4 \times 10^{20}$ cm^{-2}, which corresponds to the average over the ExSeSS area. Fluxes were estimated in the standard 0.5–2 keV band based on the medium (1–2 keV) band count rates to enable comparison with prior X-ray surveys, as well as in the 2–10 and 0.3–10 keV energy bands.[6] This differs from the way 2SXPS calculated fluxes, which used spectral fits or hardness ratios of the individual sources. We do not use the same approach as 2SXPS here as assuming a single spectral shape means that a consistent count-to-flux conversion is applied both when measuring fluxes for individual sources and when accounting for the sensitivity, as well as avoiding effects due to poorly constrained spectral properties that come from individual hardness ratios in 2SXPS. In Section 3.2 we use a more sophisticated approach to calculate the hard band fluxes, which involves adding an absorption factor calculated from the average hardness ratios.

[6]Conversion factors were calculated using the WebPIMMS tool: https://heasarc.gsfc.nasa.gov/cgi-bin/Tools/w3pimms/w3pimms.pl

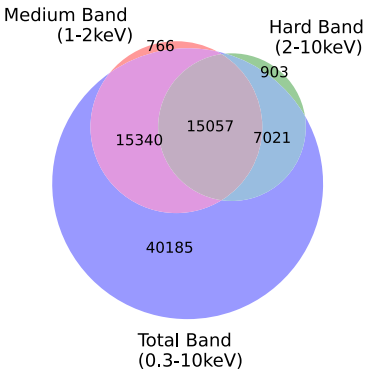

Figure 3. Venn diagram showing the number of sources that are detected in the medium (red), hard (green), and total (blue) bands, with overlapping regions indicating the numbers of sources detected in multiple bands. The total band has the largest number of sources as it has the best sensitivity but there are 766 sources detected only in the medium band and 903 sources detected only in the hard band.

Fig. 3 provides a Venn diagram showing the number of sources in the medium, hard, and total band, and the overlap between them when sources are detected in multiple bands. For example, the brown overlapping region indicates the 15 057 sources that are detected in

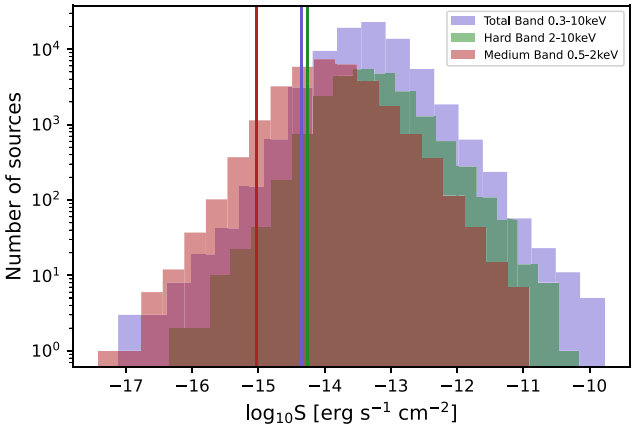

Figure 4. Distribution of fluxes for sources detected in each band. The total band (blue) has the largest number of sources covering a broad range of fluxes. The hard band (green) has more sources at brighter fluxes compared with the medium band (red) which has more sources at fainter fluxes. The solid lines show the reliable sensitivity limit at 0.1 per cent area cut-off; below this limit the area curve becomes unreliable and we thus exclude sources with fluxes fainter than this limit from our statistical analysis (see Section 3).

all three bands. Most of the ExSeSS sources are detected in the total band but there are a small number of sources that are only detected in the medium or hard bands.

Fig. 4 shows how the number of sources are distributed in each band in terms of flux, with the largest number of sources detected in the total band. In the remainder of this paper, we will mainly focus on the hard (2–10 keV) band sample as such a large sample over this flux range is unique to ExSeSS. A description of the final source catalogue is given in Appendix A, while the full catalogue is made available online.[7]

2.3 Calculation of survey area and sensitivity

A major advantage of our careful process to define the ExSeSS fields (see Section 2.2.1) is that we end up with a survey with a well-defined area coverage. Furthermore, ensuring we only retain detections in stacked data sets (where available) ensures a well-defined sensitivity over any part of the sky, allowing us to generate area curves that give the flux limit reached as a function of sky area, as shown in Fig. 5. To determine these area curves, we first calculated the sky area coverage as a function of exposure time based on the exposure maps for each of the ExSeSS fields, excluding any areas within the specified radius of targets that are also excluded in the construction of the source sample. Secondly, we calculated the fraction of sources that would be detected in areas with a given exposure time as a function of their count rate, based on the simulations described in section 7 of Evans et al. (2020). We note that these simulations were carried out assuming different source and background count rates and must be scaled to predict the detection probability in specific energy bands at a certain exposure time given knowledge of the spectral shape of the background from 2SXPS. The final step involved combining the area as a function of exposure time and the detection probability for a given exposure time to calculate the area as a function of source count rate. This process is then repeated for each band. Fig. 5 shows the resulting area curves, applying our standard conversion of rate to flux (assuming a $\Gamma = 1.9$ and Galactic absorption of $N_{\rm H} = 4 \times 10^{20}$ cm^{-2}). However, we note that the sensitivity is determined in terms of count rate which is thus independent (to first order) of the assumed X-ray spectrum.

The total area coverage is 2086.6 deg^2 making ExSeSS one of the largest, sensitive, truly serendipitous X-ray surveys to-date, especially in the hard (2–10 keV) band. For each band there is a well-defined area curve, which is needed to determine the true sky density of sources as a function of flux. The dashed line in Fig. 5 refers to where the area curve in each band goes below 0.1 per cent of its maximum value. While sources are detected with lower fluxes, below this point the simulations from Evans et al. (2020) are insufficient to accurately trace the shape of the sensitivity curve (requiring many more simulations on a much refined grid of exposure times that is computationally unfeasible) and thus we class the area curve as unreliable below this point and do not use sources below these limits in our statistical analysis (see Section 3 below).

2.4 Comparison of survey area and sensitivity with previous surveys

Fig. 6 shows how ExSeSS compares to other surveys in terms of the sky coverage as a function of the hard (2–10 keV) band flux. It shows that ExSeSS has a much greater area coverage than prior surveys and covers a range of flux and area coverage that would otherwise remain unexplored for this energy band until *eROSITA* finishes its all-sky survey, shown with the purple lines. Although *eROISTA* will cover more sky to fainter fluxes, the sample is constructed in the 2.3–5 keV band due to limited sensitivity above 5 keV, whereas ExSeSS uses the data over the full 2–10 keV range and thus corresponds to a harder energy band. Thus, ExSeSS will still access a distinct parameter space even when the full-depth *eROSITA* survey has been completed.

3 MEASUREMENTS OF X-RAY SOURCE NUMBER COUNTS

3.1 Integrated number counts, $N(>S)$, in three energy bands

One of the primary results that can be obtained from the carefully constructed ExSeSS sample is a measurement of the number count (sky density) of sources as a function of flux, known as the logN-logS. To make these measurements, we first converted the count rates into fluxes for each band, initially assuming all sources have an X-ray spectrum with $\Gamma = 1.9$ and Galactic absorption of $N_{\rm H} = 4 \times 10^{20}$ cm^{-2} only as described in Section 2.2.3.

The integrated number counts, i.e. the number of sources greater than a given flux, S, is given by

$$N(>S_j) = \sum_{i=1}^{i=M} \frac{1}{\Omega_i}, \quad (1)$$

where the sum is taken over all sources with fluxes $S_i > S_j$ and S_j is the flux of the faintest object in the bin (Mateos et al. 2008). Ω_i is the area coverage associated with source i with flux S_i, obtained from Fig. 5, and allows us to account for the changing area that our survey is sensitive to throughout our flux range. The error in the integrated number counts is given by $N(>S_j)/M^{\frac{1}{2}}$ from Poisson statistics, where M is the total number of sources with $S_i > S_j$. We have not included sources with fluxes that lie below the limit corresponding to 0.1 per cent of the total area as the area curve is likely to be unreliable below this level (see Section 2.3 above). Applying this cut removed ∼3 per cent of the sources in each band of our sample. This cut is applied to the sample for the rest of the paper. Measuring

[7] https://www.swift.ac.uk/2SXPS/exsess/

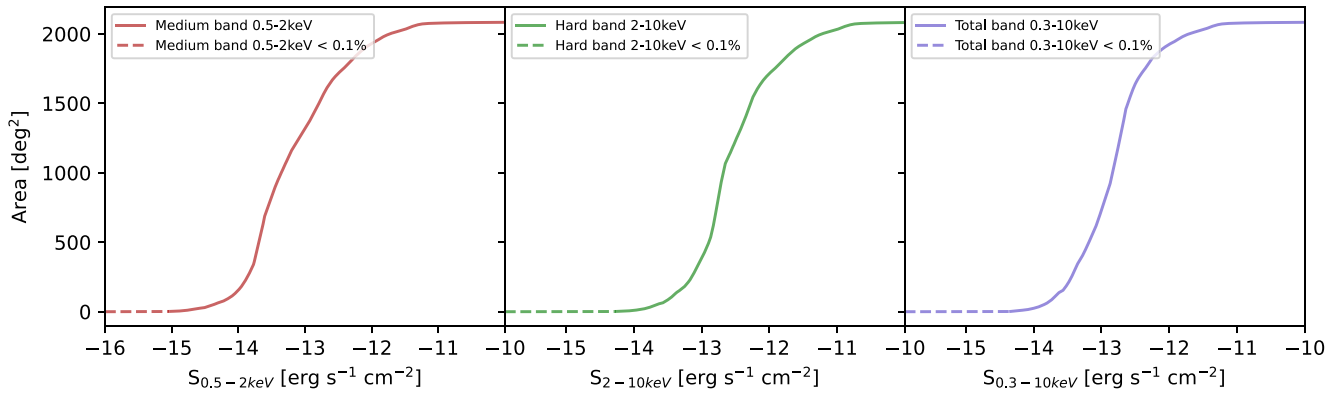

Figure 5. Area of sky covered by ExSeSS as a function of flux for the medium, hard, and total band samples. Fluxes are converted from count rates with a fixed spectral assumption (a power law with $\Gamma = 1.9$ and Galactic absorption). In the hard band, the area curve is shifted towards higher fluxes (compared to the medium or total band) due to the reduced sensitivity of the *Swift*/XRT at higher energies. We note that the medium band area curve has different shape as it is more strongly affected by the Poisson nature of the detection and the transition between photon limited and background limited regimes due to the narrower (1–2 keV) band used for the detection. The dashed lines indicate where the area drops to below 0.1 per cent of the maximum value of the area and we are no longer able to accurately determine the sensitivity from our simulations.

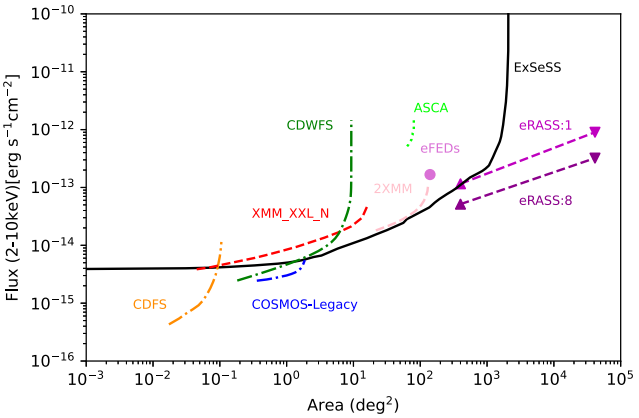

Figure 6. ExSeSS area coverage as a function of 2–10 keV flux limit (solid black line) compared with other surveys probing a similar energy flux range (curves span the flux limits achieved over 10 per cent to 90 per cent of the total area of a given survey). In red (XMM-XXL-N) and pink (2XMM) we have area coverage of two different *XMM–Newton* surveys (Mateos et al. 2008; Liu et al. 2016). Yellow (CDFS), blue (COSMOS-Legacy), and dark green (CDWFS) curves are from *Chandra* surveys (Civano et al. 2016; Luo et al. 2016; Masini et al. 2020). In lime green (ASCA) is the area coverage of the ASCA Large Sky Survey (Ueda et al. 2001, 2003, 2005; Akiyama et al. 2003). ExSeSS has a very large area when compared to these other surveys and acts as a great precursor for *eROSITA* (Sunyaev et al. 2021). The light purple point indicates the flux limit achieved in the 140 deg^2 eFEDS field (Brunner et al. 2022). The purple line (eRASS:1) is sky coverage of *eROSITA* after it first scans the whole sky (with the triangle indicating the deeper limits for the equatorial poles) and the dark purple (eRASS:8) is the sky coverage at the final depth for the full 4-yr survey. We note that *eROSITA* surveys use the 2.3–5 keV band for source detection due to limited sensitivity above 5 keV, compared with ExSeSS which uses the full 2–10 keV band.

the sky density of sources helps us to understand how the AGN population changes over different flux ranges. Fig. 7 shows the logN-logS measurements for the ExSeSS sample and compares them to fits from Georgakakis et al. (2008) and Brunner et al. (2022) and measurements from Masini et al. (2020) and Mateos et al. (2008).

The top plot of Fig. 7 shows our measurements of $N(>S)$ as a function of 0.5–2 keV flux based on our medium band (1–2 keV) selected sample, compared to previous studies. We find that the ExSeSS sample is generally in good agreement with previous measurements, although with slightly higher number densities at both the high and low ends of our flux range. We note that the measurements from the CDWFS (Masini et al. 2020) give lower number densities at bright fluxes, which could be due to the relatively small size of the field. The middle plot in Fig. 7 shows the hard (2–10 keV) band ExSeSS number counts which also lie above the 2–10 keV measurements by Masini et al. (2020) in the CDFWS and Brunner et al. (2022) in the eFEDS field but are generally in good agreement with Georgakakis et al. (2008) and Mateos et al. (2008). For the hard band, we also compare to results from MAXI (Kawamuro et al. 2018) at the bright fluxes. There is a small dip in the ExSeSS number counts at these brighter fluxes and therefore our measurements lie slightly lower than the MAXI results but are reasonably consistent. We note the relatively small range of fluxes at these harder energies probed by the early *eROSITA* final equatorial depth (eFEDS) performance verification data (Brunner et al. 2022) and that a simple extrapolation of the best-fitting power law found in that study would significantly underpredict the number counts at brighter fluxes compared to our ExSeSS measurements or the MAXI measurements. We investigate the hard band number counts in more detail, in their differential form, and compare to studies at higher energies in Section 3.3 below. Finally the bottom plot in Fig. 7 shows that there is some agreement between ExSeSS and previous measurements for the total 0.3–10 keV band with the Georgakakis et al. (2008) fit slightly overpredicting the number density and the Masini et al. (2020) measurements in good agreement with ExSeSS up to $10^{-12.5}$ erg s^{-1} cm^{-2} where ExSeSS has greater area coverage and better source statistics.

3.2 Average absorption column density as a function of flux for the hard-band ExSeSS sample

To gain a greater understanding of the underlying AGN population, we now explore the spectral properties of the ExSeSS sample and use these constraints to get more accurate values for fluxes, rather than using a simple conversion that assumes a power-law spectrum with $\Gamma = 1.9$. We focus on the hard band (2–10 keV) for the rest of this paper as such a large sample at these energies is a key feature of

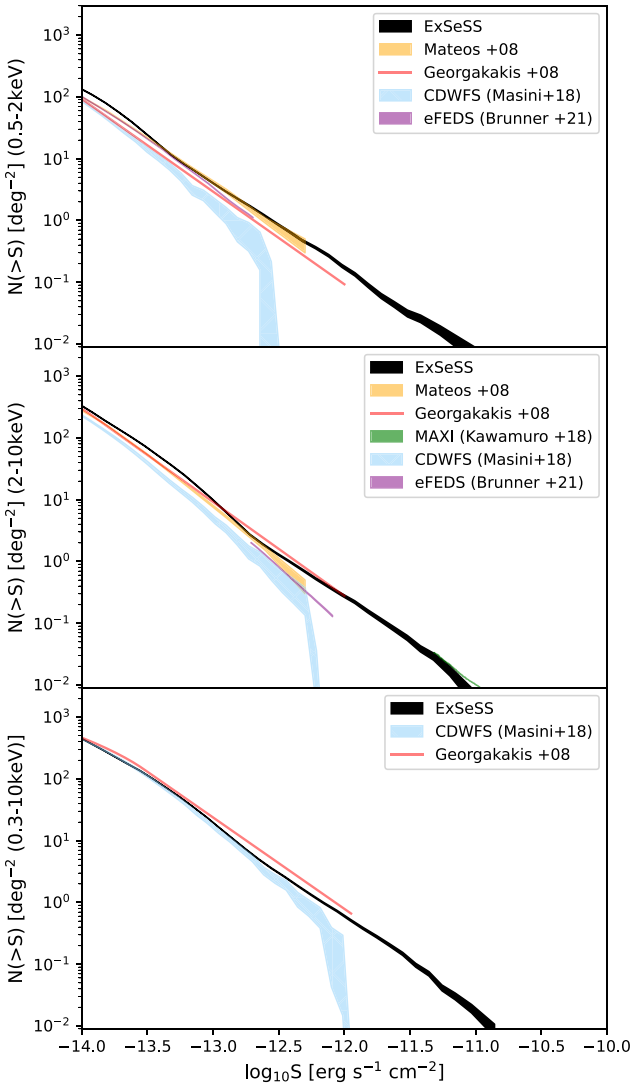

Figure 7. Integrated number counts, $N(>S)$, as a function of flux in the 0.5–2 keV (top), 2–10 keV (centre), and 0.3–10 keV (bottom) energy bands, based on the medium, hard, and full band ExSeSS samples, respectively. We compare to previous measurements with *XMM–Newton* (Mateos et al. 2008), *Chandra* (Georgakakis et al. 2008), *eROSITA* in the ∼140 deg^2 eFEDS field (Brunner et al. 2022), *Chandra* from the CDWFS (Masini et al. 2020), and MAXI (Kawamuro et al. 2018). For the medium band sample (comparing 0.5–2 keV fluxes) there is a good agreement between the results but the ExSeSS sample tends to give higher number counts below 10^{-13} erg s^{-1} cm^{-2}. In the hard band, ExSeSS agrees well with the previous results, including MAXI at very bright fluxes ($\sim 10^{11}$erg s^{-1} cm^{-2}) and is higher than the CDWFS measurements at $\sim 10^{-12.5}$ erg s^{-1} cm^{-2}. In the total band, ExSeSS is in good agreement with the CDWFS measurements (Masini et al. 2020) and lies slightly below the Georgakakis et al. (2008) best-fitting relation at brighter fluxes.

ExSeSS and substantially obscured AGN populations are more likely to be identified in this band.[8] More careful consideration of spectral properties is also necessary when comparing in detail to previous

[8]We choose not to calculate average HR and the equivalent effective $N_{\rm H}$ for the 3 per cent of hard-band sources in ExSeSS with fluxes below the 0.1 per cent area coverage limit as these faint sources tend to have poorly constrained HR values and are not included in our logN-logS measurements.

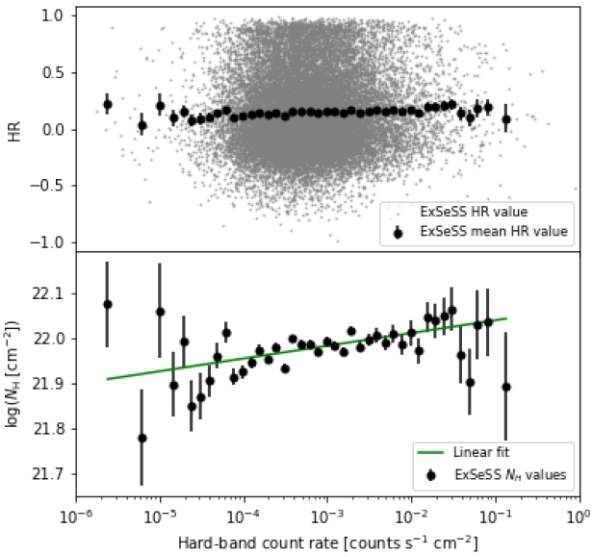

Figure 8. The first panel shows how the hardness ratio (HR) varies with rate across all of the ExSeSS sources (grey points) and the average in the pre-defined bins in hard-band count rate (black points). The second panel shows the $N_{\rm H}$ corresponding to the average HR as a function of count rate. The green line is a χ^2 fit to the data with a linear relation in log $N_{\rm H}$ − −log rate space. On average the ExSeSS hard-band sample can be described by an X-ray spectrum with $\Gamma = 1.9$ and an $N_{\rm H} \approx 10^{22}$ cm^{-2}.

measurements both in this energy band and extrapolated from higher energies (see Section 3.4 below).

To take in to account how the spectral properties change over our hard-band sample, we used the hardness ratios (HRs) provided in the 2SXPS catalogue, which were calculated using

$$HR = \frac{H - M}{H + M}, \tag{2}$$

where H is the hard band (2–10 keV) count rate and M is the medium band (1–2 keV) count rate. Given the large scatter and uncertainty in individual HR values, we binned our sources according to the hard band count rate and calculated the mean HR for each bin. The top panel of Fig. 8 shows both the individual HR values for each source (grey crosses) and the mean HR values at a given hard band rate (black circles). The error in the mean HR values are given by the standard error in the mean.

We then used WebPIMMS[9] to determine the HR that would be observed with *Swift*/XRT for a range of $N_{\rm H}$ values and a fixed $\Gamma = 1.9$ spectrum. We interpolated the above conversions to infer a mean $N_{\rm H}$ corresponding to the observed mean HR values at a given hard band count rate. Fig. 8 (lower panel) shows how the inferred $N_{\rm H}$ changes as a function of count rate, where the green line is a χ^2 fit to the data for a linear relation given by

$$\log\left(N_{\rm H}\ [\rm cm^{-2}]\right) = 0.0173 \log\left(\text{count rate}\ [\rm s^{-1}]\right) + 22.03. \tag{3}$$

We used this linear fitting relation to assign a value of $N_{\rm H}$ to each of the individual hard-band ExSeSS sources, according to their count rate. Taking an average of these values, we found that ExSeSS has a mean $N_{\rm H} = 10^{22}$ cm^{-2}. Using the values of $N_{\rm H}$ assigned to each source, along with an assumed $\Gamma = 1.9$, provides flux conversion factors that take into account the impact of absorption on the typical spectral properties of the ExSeSS sources; they should

[9]https://heasarc.gsfc.nasa.gov/cgi-bin/Tools/w3pimms/w3pimms.pl

not be interpreted as a measurement of the intrinsic absorption of the AGN spectrum that requires knowledge of the redshift. We also note that we did not find a large change in the inferred $N_{\rm H}$ values over the range of count rates that our sample covers, with the average varying by $\lesssim 0.1$ dex (see Fig. 8). None the less, accounting for the impact of absorption (with an effective $N_{\rm H} \approx 10^{22}$ cm^{-2}) on the X-ray spectral properties of our sources in this manner does improve the accuracy of our 2–10 keV flux measurements compared to our prior assumption of Galactic absorption only and thus improves the accuracy of our number counts measurements in Section 3.3 below.

3.3 Differential number counts, d*N*/d*S*, using the hard-band ExSeSS sample

Another way to analyse the X-ray source population is to determine the rate of change of the number counts as a function of flux, $\frac{\rm dN}{\rm dS}$. This allows us to more accurately diagnose the shape of the relation for comparison with previous measurements and ensures that the errors are independent at a given flux. As in Section 3.2 above, here we focus on the hard (2–10 keV) selected sample only.

Following the methods of Mateos et al. (2008), the differential number density of sources per unit flux and sky area, $n(S_j)$, are given by

$$n(S_j) = \frac{\rm dN}{\rm dS} = \frac{\sum_{i=1}^{i=m} \frac{1}{\Omega_i}}{\Delta S_j}, \quad (4)$$

where m is the number of sources in bin j with assigned flux S_j, Ω_i is the sky area coverage (in deg^2) for source i, and ΔS_j is the width of the bin in flux. The errors in $n(S_j)$ are calculated in a similar way as in Section 3.1 based on Poisson statistics, thus the error in each binned measurement is given by $n(S_i)/m^{\frac{1}{2}}$ (Mateos et al. 2008). We note that our bins are initially defined in terms of count rate. The sky area, Ω_i, is also determined depending on the count rate so that it is independent of the spectral assumption. If a bin contains less than 10 sources it is merged with the previous bin and the average count rate of sources in the combined bin is used to calculate S_j; otherwise, the central point of the bin in count rate is used to calculate S_j. Once the bins have been defined then count rates are converted to 2–10 keV fluxes assuming a spectrum with $\Gamma = 1.9$ and the variable $N_{\rm H}$, depending on the hard-band count rate, determined in Section 3.2 above.

Fig. 9 shows our measurements of $\frac{\rm dN}{\rm dS}$ normalized relative to the Euclidean slope, i.e. $\frac{\rm dN}{\rm dS} \times S^{2.5}$. Normalizing by the Euclidean slope allows for even more subtle variations to be identified between different measurements of the differential number counts that have a steep slope over this flux range. We will normalize by the Euclidean slope for all our plots of $\frac{\rm dN}{\rm dS}$. Fig. 9 compares our ExSeSS results with the double power-law fits from Georgakakis et al. (2008, based on a compilation of dedicated *Chandra* surveys) and Mateos et al. (2008, based on a well-defined subset of 2XMM). We find good agreement between ExSeSS and the Georgakakis et al. (2008) relation at faint fluxes ($S_{\rm 2-10\,keV} \sim 10^{-14} - 10^{-12.75}$erg s^{-1} cm^{-2}). At $S_{\rm 2-10\,keV} \sim 10^{-12.75} - 10^{-12.0}$erg s^{-1} cm^{-2} the differential number counts dip and agree more closely with the Mateos et al. (2008) fit before increasing again to match the Georgakakis et al. (2008) fit again at brighter fluxes (albeit with larger uncertainties in this regime). We note that the *Chandra* and *XMM–Newton* studies cover substantially smaller areas than ExSeSS and thus are dominated by sources at relatively fainter fluxes. The dot-dashed lines in Fig. 9 show where the fits have been extrapolated beyond the flux range covered by the corresponding source samples. The overall agreement between ExSeSS and these previous studies is a positive sign but the changing shape over the full flux range that we probe with ExSeSS hints that the AGN population may be more complex than previously thought. Given the high precision of ExSeSS, it is clear that a simple power law does not describe the differential number counts well in this flux regime.

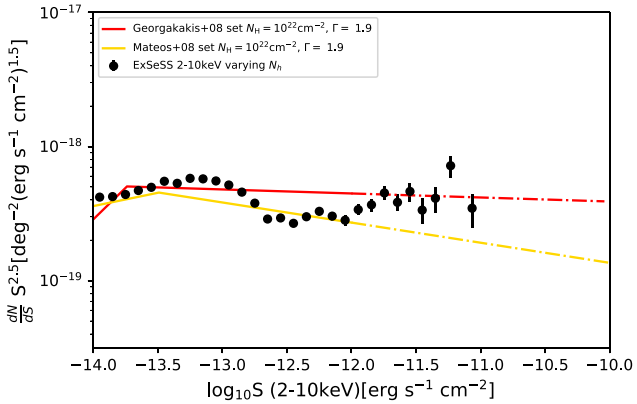

Figure 9. ExSeSS hard band (2–10 keV) sample compared with the fits from Mateos et al. (2008) using *XMM–Newton* data and Georgakakis et al. (2008) using *Chandra* data, in both cases assuming a fixed $N_{\rm H} = 10^{22}$ and $\Gamma = 1.9$ when estimating fluxes. The dot-dashed portions of the lines indicate where the best-fitting relation has been extrapolated beyond the range of fluxes probed by a given survey. ExSeSS follows similar trends as Georgakakis et al. (2008) up to $S_{\rm 2-10\,keV} \sim 10^{-12.75}$ ergs s^{-1} cm^{-2} where ExSeSS then decreases to agree more closely with the Mateos et al. (2008) fit, with good agreement at $S_{\rm 2-10\,keV} \sim 10^{-12.5} - 10^{-12.0}$ erg s^{-1} cm^{-2}. At brighter fluxes there is increased scatter in the ExSeSS measurements but they rise again to agree with the extrapolation of the Georgakakis et al. (2008) fit.

3.4 Reconciling differential number counts with measurements at higher energies

In Fig. 10 we now compare the ExSeSS differential number counts with measurements at higher energies from *NuSTAR* (at 8–24 keV: Harrison et al. 2016) and *Swift*/BAT (at 15–55 keV: Ajello et al. 2012) and investigate the impact of different spectral assumptions that are required to translate the fluxes to the 2–10 keV band. To calculate the equivalent 2–10 keV fluxes for each of the higher energy samples, we first translate the fluxes in the original energy bands back to count rates using the same spectral assumptions as the relevant study, and then calculate a new count rate to 2–10 keV flux conversion factor using our own spectral assumptions (as detailed below) to estimate the equivalent flux for comparison with the ExSeSS measurements. This process thus accounts for the differing sensitivity of a given instrument over the observed energy band and the impact of the assumed spectral model on the original flux estimates.

The top panel of Fig. 10 shows results using just a simple photon index of $\Gamma = 1.9$ (and Galactic $N_{\rm H}$ only) for the flux conversion. Under this assumption, we find that the ExSeSS measurements are well aligned with the *Swift*/BAT measurements at bright fluxes (although we note the limited overlap in flux range), whereas the *NuSTAR* measurements at fainter fluxes are significantly higher than the ExSeSS results. The discrepancy likely indicates a significant population of obscured AGN with X-ray spectra that are not well described by a simple $\Gamma = 1.9$ power law that are identified by *NuSTAR* at 8–24 keV and thus extrapolating fluxes without allowing for absorption effects leads to an overestimate of the 2–10 keV fluxes and a discrepancy in the number counts. In the second panel of Fig. 10 we instead assume an X-ray spectrum with $\Gamma = 1.48$. Harrison et al.

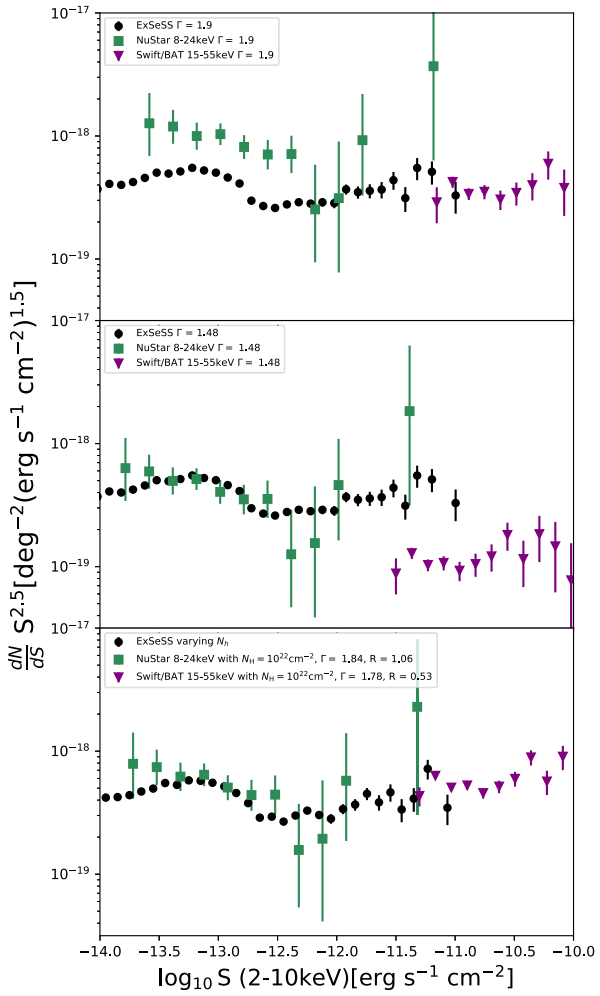

Figure 10. The top panel is a comparison of the ExSeSS sample to the *NuSTAR* 8–24 keV and *Swift*/BAT 15–55 keV surveys (Harrison et al. 2016) using a underlying spectral assumption of single power law with a photon index of $\Gamma = 1.9$. The middle panel is a similar comparison as in the first one but using a fixed $\Gamma = 1.46$ and therefore assuming we are observing a less obscured population for *NuSTAR* and *Swift*/BAT. Using a variable $N_{\rm H}$ for ExSeSS and the correct underlying spectral properties for *NuSTAR* and *Swift*/BAT gives a much better agreement between the ExSeSS sample and the previous results when compared with just using a simple photon index as shown in the bottom panel.

(2016) found that this flatter spectral shape, allowing for the presence of absorbed sources, was needed to bring the *NuSTAR* 8–24 keV number counts into good agreement with previous, lower energy measurements with *Chandra* and *XMM–Newton*. With this same spectral assumption, we find good agreement between the ExSeSS[10] and *NuSTAR* measurements at fluxes $\sim 10^{-14}$–10^{-12} erg s^{-1} cm^{-2}, whereas at brighter fluxes there is now a significant offset between ExSeSS and the *Swift/BAT* measurements. We thus conclude that there are significant differences in the underlying X-ray spectral properties of the source samples selected by ExSeSS, *NuSTAR*, and *Swift*/BAT at different flux and energy ranges such that a single spectral assumption is insufficient to reconcile measurements of the differential number counts.

In the bottom panel of Fig. 10 we present the ExSeSS measurements using a variable $N_{\rm H}$ as described in Section 3.2 as well as using the *observed* spectral properties of the *NuSTAR* and *Swift*/BAT samples when converting from the measured energy range to 2–10 keV. For NuSTAR we adopt $\Gamma = 1.84$, $N_{\rm H} = 10^{22}$ cm^{-2}, $z = 0.58$ and include a reflection component (modelled using PEXRAV) with a relative normalization of $R = 1.06$, based on the mean of the parameters determined from spectral analysis of the *NuSTAR* 8–24 keV selected sample by Zappacosta et al. (2018). For *Swift*/BAT we adopt $\Gamma = 1.78$, $N_{\rm H} = 10^{22}$ cm^{-2}, and a reflection component with $R = 0.53$, based on the mean values from the spectral analysis by Ricci et al. (2017). Conversion factors to translate fluxes between energy bands, assuming the above parameters, were calculated using XSpec.[11] We note that our method adopts a single spectral assumption for *all* sources in a given high-energy sample, while in reality there will be a distribution of properties across the population that may have second-order effects on the extrapolated 2–10 keV differential number counts. None the less, using this method we obtain a good agreement between ExSeSS, *NuSTAR*, and *Swift*/BAT, in contrast to the results shown in the top and middle panels that assumed a single photon index showing how important it is to take into account the underlying spectral properties of the sources identified by different surveys when comparing measurements of the number counts. Our approach means that we adopt the closest spectral properties to the population probed in a given sample, but we have not further tuned other parameters to make the different samples agree with each other.

It is interesting to note that the spectral parameters are different for *NuSTAR* and *Swift*/BAT with *Swift*/BAT sources typically having half the reflection component of NuSTAR and the photon index differing by 0.06 hinting at differences in the AGN population identified at higher energies in different flux ranges. Applying the appropriate flux conversions brings the *Swift*/BAT and *NuSTAR* measurements of differential number counts into good agreement with our measurements with ExSeSS.

3.5 Comparison with AGN population synthesis models

Fig. 11 shows how the differential number counts of ExSeSS and *Swift*/BAT sample compare with the predictions of population synthesis models from Ueda et al. (2014); Gilli et al. (2007) and Ballantyne (2014, as updated in Harrison et al. 2016). As in Sections 3.3 and 3.4 above, we adopt the variable (count rate dependent) estimates of $N_{\rm H}$ when determining the ExSeSS fluxes as detailed in Section 3.2. The population synthesis models account for the diverse range of spectral properties (i.e. a range of absorption columns, redshifts, and luminosities) in the underlying AGN population when predicting the number counts as a function of 2–10 keV flux, enabling a direct comparison to our ExSeSS measurements.

There is good agreement between ExSeSS and the Gilli et al. (2007) model at the faint end of our flux range ($\lesssim 10^{-13.5}$ erg s^{-1} cm^{-2}) and over the flux range 10^{-14} – 10^{-12} erg s^{-1} cm^{-2} the ExSeSS measurements are broadly consistent with the model predictions, although the differential number counts of ExSeSS vary much more over this flux range, similar to as seen in Fig. 9 comparing with Mateos et al. (2008); Georgakakis et al. (2008) power-law fits. There are thus hints from ExSeSS that there is more

[10]For consistency, we also assume $\Gamma = 1.48$ when calculating the ExSeSS source fluxes, although this change has a minimal impact given the count rates are measured in the same 2–10 keV band used for the flux.

[11]https://heasarc.gsfc.nasa.gov/xanadu/xspec/

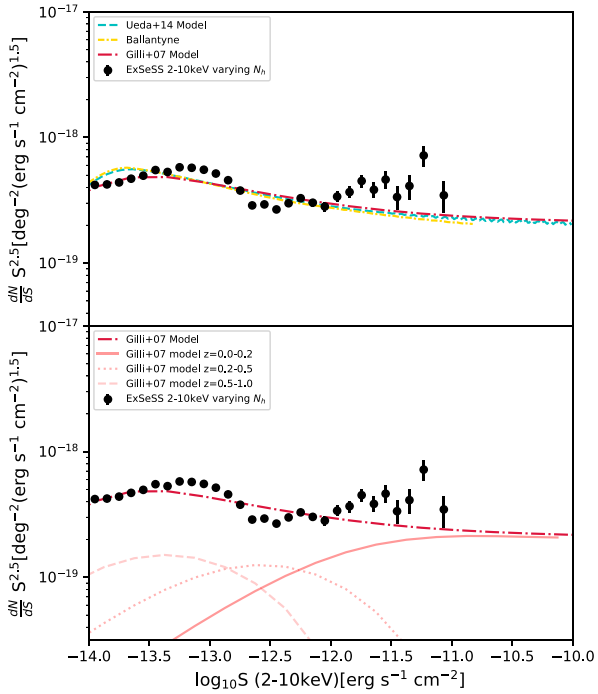

Figure 11. Top panel: Comparison of the differential number counts of the ExSeSS sample using the variable $N_{\rm H}$ method from Section 3.2 and the population synthesis models from Ueda et al. (2014); Gilli et al. (2007) and Ballantyne (2014, as updated in Harrison et al. 2016). There is a generally good agreement between the ExSeSS sample and the different models (Gilli et al. 2007; Ueda et al. 2014) and Ballantyne over the flux range $10^{-14} - 10^{-12}$ erg s^{-1} cm^{-2} and between ExSeSS and Gilli et al. (2007) for values $<10^{-13.5}$ erg s^{-1} cm^{-2}. At the bright end the models and ExSeSS start to diverge at values $>10^{-12}$ erg s^{-1} cm^{-2}. Bottom panel: comparison of the ExSeSS measurements and contributions to the Gilli et al. (2007) model from AGN over different redshift ranges (solid, dotted, and dashed pink lines corresponding to the indicated redshifts). At bright fluxes $>10^{-12}$ erg s^{-1} the number counts are dominated by low redshift sources with $z = 0.0 - 0.2$. This is where our main discrepancy lies and ExSeSS hints at a population of AGN at these lower redshifts that is not accounted for in the current models.

variation in the differential number counts of the AGN population over this flux range than the models are currently predicting.

At high fluxes ($\gtrsim 10^{-12}$ erg s^{-1} cm^{-2}), the measurements indicate that there are substantially more AGNs than the models currently predict meaning they need to be updated over this flux regime. This discrepancy could be due to the fact that at 2–10 keV energies at these fluxes we are detecting more AGNs than predicted by the models, which are primarily constrained by surveys probing fainter flux regimes and lower energies. To investigate further, in the lower panel of Fig. 11 we show the contributions to the Gilli et al. (2007) model from AGN in different redshift ranges. It is clear that at bright fluxes ($\gtrsim 10^{-12}$ erg s^{-1} cm^{-2}) the model is dominated by low redshift sources, $z = 0.0 - 0.2$. It is thus likely that ExSeSS is picking up a population of AGN at these redshifts which the models do not currently take into account. Harrison et al. (2016) also showed that there is a discrepancy between the *NuSTAR* 8–24 keV results and the *Swift*/BAT 15–55 keV results (converted to the 8–24 keV band) as well as showing a discrepancy between the data and the models and suggested that updates are required to the population synthesis models at lower redshifts. However, Harrison et al. (2016) found that the models overpredict the *Swift*/BAT number counts, whereas here we find that the models are underpredicting compared to our ExSeSS measurements at 2–10 keV. Overall our results indicate that the population synthesis models may need updating to accurately account for this population of AGN identified at 2–10 keV energies over this flux range.

An alternative explanation for the increase in the ExSeSS number counts at bright fluxes compared to the AGN population synthesis models could be due to the presence of a contaminating, non-AGN population of sources. Without multiwavelength associations or classifications (deferred to the next stage of our study), we are unable to classify individual X-ray sources directly. However, by extrapolating the number counts of different populations (AGN, galaxies, and stars) measured in the CDFS by Lehmer et al. (2012), we can estimate the expected level of contamination. At a 2–10 keV flux of $S = 10^{-12.5}$ erg s^{-1} cm^{-2} (the lowest point of the ExSeSS sample in Fig. 11) we measure a value of $\frac{{\rm d}N}{{\rm d}S} S^{2.5} \approx 3 \times 10^{-19}$ deg^{-2} (erg s^{-1} cm^{-2})$^{1.5}$. Extrapolating the power-law fits from Lehmer et al. (2012) for the 2–8 keV band to the same flux predicts a value of $\approx 7.4 \times 10^{-21}$ for stars, $\approx 2.1 \times 10^{-21}$ for galaxies and $\approx 2.6 \times 10^{-19}$ for AGN. The number counts values we get for our sample agree well with the Lehmer et al. (2012) numbers counts for AGN whereas the galaxy and star number counts are significantly lower suggesting these populations do not substantially contaminate our sample and gives us great confidence that the ExSeSS sample is dominated by AGN. It also suggests that the up-turn in our number counts measurements at bright fluxes is not caused by any star or galaxy contribution.

4 SUMMARY AND CONCLUSIONS

In this paper we presented the new X-ray source catalogue for the ExSeSS sample detected in the medium (1–2 keV), hard (2–10 keV), and total (0.3–10 keV) energy bands. We use this sample to calculate the number density of sources as a function of flux, providing new constraints on the AGN population. The main points to take away from this paper are:

(i) Based on the most recent compilation of point sources detected by the *Swift*/XRT between 2005 January 1–2018 August 1 (2SXPS: Evans et al. 2020), we have defined the ExSeSS sample with a total of 79 342 unique X-ray sources. Our sample includes sources detected in the 1–2 keV (medium), 2–10 keV (hard), and 0.3–10 keV (total) energy ranges and has a total sky coverage of $\sim$2086.6 deg^2 over the flux range of $\sim 10^{-14} - 10^{-11}$erg s^{-1} cm^{-2}. This is a previously unexplored parameter space where the ExSeSS sample can place unprecedented constraints on the X-ray source population.

(ii) We compared the number counts based on the ExSeSS sample as a function of flux in the hard (2–10 keV) and total (0.3–10 keV) energy bands as well the 0.5–2 keV band (derived from the medium 1–2 keV detections) to previous results and fits shown in Fig. 7. There is a generally good agreement between ExSeSS and previous results, although we measure consistently higher number counts than prior studies in the medium band. We generally found good agreement with previous estimates in the hard band, although our measurements are slightly higher than Masini et al. (2020) and Brunner et al. (2022). In the total band, our measurements provide accurate measurements over a wide range in flux and are in good agreement with previous measurements.

(iii) We also compared measurements of differential number counts (dN/dS) from ExSeSS to previous fitted relations in the 2–10 keV band derived from *Chandra* (Georgakakis et al. 2008) and *XMM–Newton* (Mateos et al. 2008) (see Fig. 9). Our measurements are broadly in agreement with these prior fits between 10^{-14} and

10^{-12} erg s^{-1} cm^{-2} although our measurements show the differential number counts are not well described by a single power law over this flux range. Furthermore, at fluxes $>10^{-12}$ erg s^{-1} cm^{-2} (where ExSeSS covers an unprecendented area compared to prior *Chandra* and *XMM–Newton* surveys) we see a rise in the number counts in comparison to an extrapolation of the Mateos et al. (2008) fit, again showing that a power-law distribution does not adequately describe the AGN number counts over this broad range of fluxes.

(iv) We found a good agreement between our ExSeSS measurements of 2–10 keV differential number counts and extrapolations from previous higher energy surveys (*NuSTAR* and *Swift*/BAT) provided that we adopt appropriate and realistic spectral models for each sample when converting to 2–10 keV fluxes. We also require different spectral models to reconcile both the *NuSTAR* 8–24 keV measurements at lower fluxes and the *Swift*/BAT 15–55 keV measurements at higher fluxes with our ExSeSS 2–10 keV measurements, indicating there are differences in the underlying AGN populations probed by these different surveys.

(v) Comparing the hard band (2–10 keV) differential number counts to the predictions from AGN population synthesis models, we found that the ExSeSS measurements have a different shape than the model predictions. In particular, we found an excess in the differential number counts at fluxes $>10^{-12}$ erg s^{-1} cm^{-2} with ExSeSS suggesting that there is an additional population of sources detected at harder (>2 keV) energies, likely predominantly at lower redshifts ($z \lesssim 0.2$), contributing to the number counts at bright fluxes that is not fully accounted for in current population synthesis models. This contribution corresponds to nearly twice the number density compared to that predicted by the AGN population synthesis models at the brightest fluxes covered by ExSeSS. Hence these models may require updating over this flux range.

ExSeSS provides a new serendipitous sample of X-ray sources selected at the 0.3–10, 1–2, and 2–10 keV energies with a total of 79 342 unique sources and an area coverage of 2086.6 deg^2. We have used this sample to provide new constraints on the logN-logS of X-ray sources and compared these to results from other surveys performed by different telescopes, as well as comparing to the predictions of AGN population synthesis models. Comparing to other surveys we can see how the ExSeSS sample with its hard 2–10 keV sensitivity and large sky coverage over the flux range of $\sim 10^{-14} - 10^{-11}$ erg s^{-1} cm^2, as shown in Fig. 6, can provide new constraints on the AGN population.

The definition of ExSeSS in this paper represents an important first step towards future studies of this new, well-defined sample of X-ray sources. In a future study, we will perform a statistical cross-match to identify counterparts to our X-ray sources at mid-infrared wavelengths (using data from *WISE*: Wright et al. 2010) and optical wavelengths (using the Legacy Survey 8: Duncan 2022). This will provide reliable multiwavelength counterparts, enabling photometric redshift estimates, and allow us to study physical properties such as the spectral properties of the AGN, obscuration properties, and host galaxy properties for a large fraction of this sample. An SDSS-V (Kollmeier et al. 2017) open-fibre programme is also underway, providing spectroscopic follow-up of the brightest sources in our hard-band sample. Finally, we highlight work by Barlow-Hall et al. (2022) using one of the sources in our ExSeSS sample that coincides with a previously known, spectroscopically identified AGN at $z = 6.31$, combined with our well-defined survey sensitivity and coverage, to place constraints on the X-ray luminosity function of AGN at $z = 5.7 - 6.4$ and demonstrating the power and utility of ExSeSS.

ACKNOWLEDGEMENTS

We thank the referee for helpful comments that improved this paper. This work made use of data supplied by the UK Swift Science Data Centre at the University of Leicester. JD and CBH acknowledge support from STFC studentships. JA acknowledges support from a UKRI Future Leaders Fellowship (grant code: MR/T020989/1). PAE acknowledges UKSA support. For the purpose of open access, the authors have applied a Creative Commons Attribution (CC BY) licence to any Author Accepted Manuscript version arising from this submission.

DATA AVAILABILITY

ExSeSS is based on the 2SXPS catalogue (Evans et al. 2020), available at https://www.swift.ac.uk/2SXPS/ which provides full access to the underlying X-ray data products. The refined sample presented here is made available as an online catalogue with this paper and through the 2SXPS website.

REFERENCES

Aird J., Coil A. L., Georgakakis A., Nandra K., Barro G., Pérez-González P. G., 2015, MNRAS, 451, 1892
Ajello M., Alexander D., Greiner J., Madejski G., Gehrels N., Burlon D., 2012, ApJ, 749, 21
Akiyama M., Ueda Y., Ohta K., Takahashi T., Yamada T., 2003, ApJS, 148, 275
Alexander D. et al., 2013, ApJ, 773, 125
Alexander D. M. et al., 2003, AJ, 126, 539
Ballantyne D., 2014, MNRAS, 437, 2845
Barlow-Hall C. L., Delaney J., Aird J., Evans P. A., Osborne J. P., Watson M. G., 2022, preprint (arXiv:2201.11139)
Barthelmy S. D. et al., 2005, Space Sci. Rev., 120, 143
Boller T., Freyberg M., Trümper J., Haberl F., Voges W., Nandra K., 2016, A&A, 588, A103
Brandt W., Alexander D., 2015, A&AR, 23, 1
Brown J.S, Stanek K.Z., Holoien T.W.S., Kochanek C.S., Shappee B.J., Prieto J.L., Dong S., et al., 2019, MNRAS, 48, 3785.
Brunner H. et al., 2022, A&A, 661, A1
Civano F. et al., 2015, ApJ, 808, 185
Civano F. et al., 2016, ApJ, 819, 62
Duncan K. J., 2022, MNRAS, 512, 3662
Evans I. N. et al., 2010, ApJS, 189, 37
Evans P. et al., 2020, ApJS, 247, 54
Georgakakis A., Nandra K., Laird E., Aird J., Trichas M., 2008, MNRAS, 388, 1205
Gilli R., Comastri A., Hasinger G., 2007, A&A, 463, 79
Harrison F. A. et al., 2013, ApJ, 770, 103
Harrison F. et al., 2016, ApJ, 831, 185
Hickox R. C., Alexander D. M., 2018, ARA&A, 56, 625
Kawamuro T. et al., 2018, ApJS, 238, 32
Kocevski D. D. et al., 2018, ApJS, 236, 48
Kollmeier J. A. et al., 2017, preprint (arXiv:1711.03234)
Laird E. S. et al., 2009, ApJS, 180, 102
Lansbury G. B. et al., 2017, ApJ, 836, 99
Lehmer B. D. et al., 2012, ApJ, 752, 46
Liu Z. et al., 2016, MNRAS, 459, 1602
Luo B. et al., 2016, ApJS, 228, 2
Madsen K. K. et al., 2015, ApJS, 220, 8
Masini A. et al., 2018, ApJ, 867, 162
Masini A. et al., 2020, ApJS, 251, 2
Mateos S. et al., 2008, A&A, 492, 51
Merloni A. et al., 2012, preprint (arXiv:1209.3114)
Mullaney J. R. et al., 2015, ApJ, 808, 184
Nandra K. et al., 2015, ApJS, 220, 10

Netzer H., 2015, ARA&A, 53, 365
Oh K. et al., 2018, ApJS, 235, 4
Pierre M. et al., 2016, A&A, 592, A1
Predehl P. et al., 2021, A&A, 647, A1
Ricci C. et al., 2017, ApJS, 233, 17
Rosen S. et al., 2016, A&A, 590, A1
Sunyaev R. et al., 2021, A&A, 656, A132
Trümper J., 1982, Adv. Space Res., 2, 241
Ueda Y., Akiyama M., Hasinger G., Miyaji T., Watson M. G., 2014, ApJ, 786, 104
Ueda Y., Akiyama M., Ohta K., Miyaji T., 2003, ApJ, 598, 886
Ueda Y., Ishisaki Y., Takahashi T., Makishima K., Ohashi T., 2001, ApJS, 133, 1
Ueda Y., Ishisaki Y., Takahashi T., Makishima K., Ohashi T., 2005, ApJS, 161, 185
Voges W. et al., 2000, Int. Astron. Un. Circ., 7432, 3
Watson M. G. et al., 2009, A&A, 493, 339
Webb N. et al., 2020, A&A, 641, A136
Wright E. L. et al., 2010, AJ, 140, 1868
Xue Y. Q. et al., 2011, ApJS, 195, 10
Zappacosta L. et al., 2018, ApJ, 854, 33
Zheng X. C. et al., 2017, ApJ, 849, 127

SUPPORTING INFORMATION

Supplementary data are available at *MNRAS* online.

ExSeSS_sample.csv

Please note: Oxford University Press is not responsible for the content or functionality of any supporting materials supplied by the authors. Any queries (other than missing material) should be directed to the corresponding author for the article.

APPENDIX A: SOURCE CATALOGUE

Table A1 describes the final source catalogue of the ExSeSS sample with all the relevant columns. A value of −999.0 is used where there is no information on the source in that particular band.

Table A1. Information on the columns in the ExSeSS sample including IDs from original 2SXPS data (Evans et al. 2020) being the 2SXPS_ID, ObsID, RA, Decl, and all the rate and their error columns. New columns unique to ExSeSS are the fluxes and their errors where we have the medium, hard, and total converted with a simple power law of $\Gamma = 1.9$ and the hard band converted with a variable column density with a $\Gamma = 1.9$. We include the effective $N_{\rm H}$ values used to make the conversions for each flux value in the hard band. The value of −999.0 has been set for when we do not have information on the sources.

ExSeSS column descriptions

Column name	Description	Units
ExSeSS_ID	The ID of unique sources in the ExSeSS sample	–
2SXPS_ID	Source ID from the 2SXPS catalogue	–
ObsID	Data set/field ID from the original 2SXPS catalogue	–
RA	The right ascension of the source position	degrees
RA_pos	The positive error in right ascension of the source position	degrees
RA_neg	The negative error in right ascension of the source position	degrees
Decl	The declination of the source position	degrees
Decl_pos	The positive error in declination of the source position	degrees
Decl_neg	The negative error in declination of the source position	degrees
Medium_Rate	The rate for the medium 1–2 keV band	counts s^{-1}
Medium_Rate_pos	The error in the rate for the medium 1–2 keV band	counts s^{-1}
Medium_Rate_neg	The error in the rate for the medium 1–2 keV band	counts s^{-1}
Hard_Rate	The rate for the hard 2–10 keV band	counts s^{-1}
Hard_Rate_pos	The error in the rate for the hard 2–10 keV band	counts s^{-1}
Hard_Rate_neg	The error in the rate for the hard 2–10 keV band	counts s^{-1}
Total_Rate	The rate for the total 0.3–10 keV band	counts s^{-1}
Total_Rate_pos	The error in the rate for the total 0.3–10 keV band	counts s^{-1}
Total_Rate_neg	The error in the rate for the total 0.3–10 keV band	counts s^{-1}
Medium_Area	The corresponding area coverage to the source rate value in the medium band	deg^2
Hard_Area	The corresponding area coverage to the source rate value in the hard band	deg^2
Total_Area	The corresponding area coverage to the source rate value in the total band	deg^2
Soft_Flux	The flux for the soft 0.5–2 keV band estimated from the medium (1–2 keV) band rate	erg s^{-1} cm^{-2}
Soft_Flux_pos	The error in the flux for the soft 0.5–2 keV band estimated from the medium (1–2 keV) band rate	erg s^{-1} cm^{-2}
Soft_Flux_neg	The error in the flux for the soft 0.5–2 keV band estimated from the medium (1–2 keV) band rate	erg s^{-1} cm^{-2}
Hard_Flux	The flux for the hard 2–10 keV band	erg s^{-1} cm^{-2}
Hard_Flux_pos	The error in the flux for the hard 2–10 keV band	erg s^{-1} cm^{-2}
Hard_Flux_neg	The error in the flux for the hard 2–10 keV band	erg s^{-1} cm^{-2}
Total_Flux	The flux for the total 0.3–10 keV band	erg s^{-1} cm^{-2}
Total_Flux_pos	The error in the flux for the total 0.3–10 keV band	erg s^{-1} cm^{-2}
Total_Flux_neg	The error in the flux for the total 0.3–10 keV band	erg s^{-1} cm^{-2}
Effective $N_{\rm H}$	The effective column density for the hard band sample (for sources with fluxes above the 0.1 per cent area covereage cut)	cm^{-2}
Hard_Flux_variable_N_h	The flux values in the 2–10 keV band calculated using the variable, effective $N_{\rm H}$ as described in Section 3.2 with the same 0.1 per cent area cut off applied	erg s^{-1} cm^{-2}

This paper has been typeset from a TEX/LATEX file prepared by the author.